Redox-Driven Nanoscale Topotactic Transformations in Epitaxial $SrFe_{0.8}Co_{0.2}O_{3-x}$ under Atmospheric Pressure

Joonhyuk Lee,[1] Eunyoung Ahn,[1] Yu-Seong Seo,[2] Younghak Kim,[3] Tae-Yeol Jeon,[3] Jinhyung Cho,[4] Inwon Lee,[5] and Hyoungjeen Jeen[1,*]

[1] *Department of Physics, Pusan National University, Busan 46241, Korea*
[2] *Department of Physics, Sungkyunkwan University, Suwon 16419, Korea*
[3] *Pohang Accelerator Laboratory, Pohang 37673, Korea*
[4] *Department of Physics Education, Pusan National University, Busan 46241, Korea*
[5] *Department of Naval Architecture and Ocean Engineering, Pusan National University, Busan 46241, Korea*

(Received 11 July 2018; revised manuscript received 23 September 2018; published 15 November 2018)

Oxygen ion exchanges at the surface of transition metal oxides have been extensively studied for understanding their nanoscale ionic behavior as well as for realizing multifunctionalities such as exotic magnetism, insulator-to-metal transition, band gap tuning, etc. To activate this exchange behavior, in many cases extreme conditions such as high temperature, high electric fields, and high vacuum are often required. These conditions have blocked the promising materials from being applied on real devices such as solid-oxide fuel cells and other electrochemical devices. In this article, we show that redox-driven reversible topotactic transformation in epitaxial $SrFe_{0.8}Co_{0.2}O_{3-x}$ thin films can be achieved at low temperature and at atmospheric pressure. This transformation triggers changes in electronic structures as well. These reversible redox reactions and/or associated changes at low temperature and under atomospheric pressure are particularly needed to develop a cathode for low solid-oxide fuel cells.

DOI: 10.1103/PhysRevApplied.10.054035

I. INTRODUCTION

Transition metal oxides (TMOs) have been attracting much attention because of their various physical properties [1–7]. There have been many attempts to control these properties via mechanical stress, magnetic fields, electric fields, etc. Recently, control of the materials' chemistry in a reversible manner has been proposed as an active method by which to control the TMOs' physical properties [8–11]. In oxides, control of the oxygen content is a viable method for tuning the physical properties, since the number of oxygen vacancies can be controlled by a gas environment and/or by electric fields [12–15]. Among many oxides, topotactic oxides, which can vary their crystal structure under the change of the oxygen content, can be considered as promising materials for this reversible manipulation, since they do not create defects in a random fashion.

Even though the redox reactions, which are closely related to the control of the oxygen content, have recently been considered as an important way to control the physical properties in TMOs, the fundamental importance of the redox reactions in TMOs lies in energy applications [16]. Among many applications, solid-oxide fuel cells rely heavily on ion diffusion and oxygen reduction reaction processes, which are closely related to the redox reactions. In this regard, TMOs with their relatively high ionic and electronic conductivities have been actively studied for several decades as replacements for precious platinum cathodes, since the function of a cathode such as the oxygen reduction reaction is believed to determine the efficiency of solid-oxide fuel cells [17]. In solid-oxide fuel cells, one of the critical issues is lowering the working temperature from 700 °C or higher to increase the efficiency and to lower thermal degradation and costs [18]. Thus, a cathode should work properly at this lowered temperature. Recently, several redox-active topotactic oxides at low temperatures have been proposed [9,19]. The results show the materials are promising for solid-oxide fuel cells. For redox-driven topotactic transformation, these materials have required special chemicals and/or moderate vacuum levels up until now. If the conditions such as the atmospheric conditions at low temperature for the redox reaction are improved, they can be even more promising as potential cathode materials.

In this research, we observe reversible changes of the oxygen content in an epitaxially stabilized $SrFe_{0.8}Co_{0.2}O_{3-x}$ (SFCO) thin film on a (001) $(LaAlO_3)_{0.3}$-$(SrAl_{0.5}Ta_{0.5}O_3)_{0.7}$ (LSAT) substrate by varying the gas species at atmospheric pressure as well as lowering the temperature through topotactic transformation. It is expected that the

*hjeen@pusan.ac.kr

choice of a solid solution may result not only in diverse structures, but also in differences in the electronic and magnetic properties [20,21]. From real-time x-ray scattering (XRS) techniques, we show the change of gas type from air to N_2 or vice versa, which leads to transitions between an oxygen-deficient perovskite structure and a brownmillerite structure. With the use of *ex situ* probes such as x-ray absorption spectroscopy (XAS) and spectroscopic ellipsometry, we not only confirm the changes in valence state of transition metals associated with changes in the oxygen content, but also point out the reversible change of the direct optical band gap energy by about 0.5 eV upon undergoing these reversible oxygen exchanges, possibly due to the small difference in Gibbs free energies between the brownmillerite and perovskite phases.

II. EXPERIMENTAL METHODS

A. Thin-film synthesis

The epitaxial SFCO thin films are deposited on the (001) LSAT substrates by pulsed laser deposition (PLD) with a Q-switched Nd:YAG ($\lambda = 355$ nm) laser. The laser energy density and repetition rate are kept at 0.75 J/cm^2 and 4 Hz, respectively. Growth of perovskite SFCO (P-SFCO) films is conducted at 550–700 °C and 1–200 mTorr of oxygen. We find that 600 °C and 100 mTorr of oxygen partial pressure ($P(O_2)$) to be the optimal growth conditions. After deposition, thin films are cooled down to 50 °C while $P(O_2)$ in cooling is same as growth $P(O_2)$ to form an oxygen-deficient perovskite structure.

B. X-ray scattering experiments

With this as-grown thin film, real-time XRS ($\lambda = 1.240$ Å) in 3D beamline in the Pohang accelerator laboratory (PAL) is performed. First, temperature-dependent real-time x-ray diffraction (XRD) experiments are performed under reducing conditions by purging the heating chamber with N_2 gas. After confirming a complete phase transformation to the brownmillerite structure at 375 °C, real-time XRD and x-ray reflectometry (XRR) experiments are performed under oxidizing and reducing conditions: the reducing condition by using N_2 and the oxidizing condition by supplying dry air (80% N_2, 20% O_2). Even if a reversible transformation in a topotactic oxide appears, the aging effect has not been completely ruled out.

C. X-ray absorption spectroscopy and optical spectroscopy

To check the electronic properties and valence state information of transition metals, we prepare the reduced SFCO in the same reactor. XAS of Fe and Co L edge and O K edge spectra from 2A beam line, Pohang acclerator laboratory (PAL), and spectroscopic ellipsometry (J. A. Woollam Co.) are performed and analyzed with these samples.

III. RESULTS AND DISCUSSION

Epitaxial SFCO thin films are deposited on the (001) LSAT substrates by PLD. To observe the direct evidence of reduction-driven structural phase transition at low temperature, we perform real-time XRD as a function of temperatures from room temperature (RT) to 375 °C by purging the heating chamber with N_2 gas. Figure 1(a) clearly shows that discrete structural phase transformation takes place at a temperature as low as 200 °C. The half-order peak from the reduced film provides clear evidence for the formation of the brownmillerite structure, since brownmillerite consists of stacks of alternating tetrahedral layers and octahedral layers. In addition, we obtain reciprocal space maps of both cases, such as the reduced brownmillerite SFCO (BM-SFCO) and as-grown oxygen-deficient P-SFCO, as seen in Figs. 1(b) and (c). They are visualized by lattice expansion along the out-of-plane direction. We calculate that the lattice constant along the out-of-plane direction of the P-SFCO is 3.9 Å; however, after loss of oxygen atoms in the lattices, the lattice constant of the reduced film on the basis of the perovskite unit cell is 4.0 Å. It is worth noting that the in-plane lattice constants are fully locked. After showing complete phase conversion under a reducing condition, it is worth mentioning how the structure is transformed as a function of temperature. We can separate the structure into three regions based on temperature: RT to 175 °C, 175 °C to 200 °C, and 200 °C to 375 °C, which is the highest temperature in this real-time measurement. In the first region, the structure of the as-grown P-SFCO is maintained as an oxygen-deficient perovskite structure. In this region, we do not observe any clear evidence of the formation of brownmillerite structure, which can be evidence of oxygen de-intercalation. We only observe the thermal expansion of

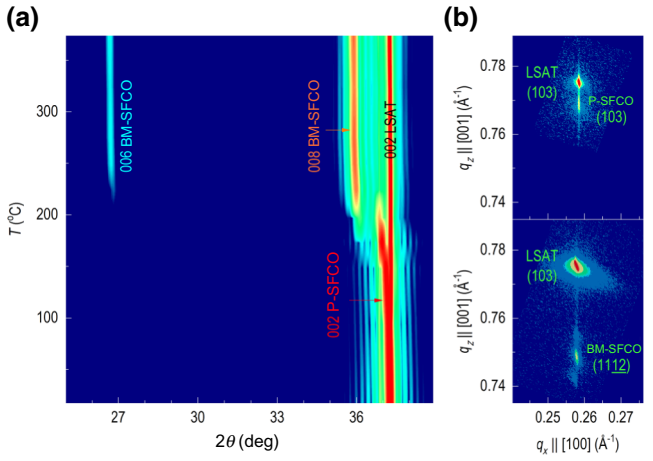

FIG. 1. (a) Temperature-dependent XRD θ-2θ measurements under ambient N_2 gas. Reciprocal space maps from (b) as-grown P-SFCO and (c) reduced BM-SFCO films under N_2 environment around the 103 LSAT Bragg reflection.

the lattice. The second region shows that new peaks form. As the new peaks appear, the peak intensity of the perovskite structure decreases. When it enters this region, the formation of the brownmillerite phase is clearly seen from the half-order peak and another peak near the substrate. Therefore, two phases, such as oxygen-deficient perovskite and brownmillerite structures, coexist. This similar coexistence of structural phases has been captured in similar materials [10]. After complete reduction takes place, we only observe the diffraction pattern corresponding to the brownmillerite phase above 225 °C. This complete reduction is likely to originate from the nature of its mother phases such as $SrFeO_x$ and $SrCoO_x$. The Gibbs free energy differences in these oxides are particularly lower at the low temperature, so this moderate gas condition can trigger the phase conversion at around 200 °C [9,20].

From the structural characterization using real-time XRD, we observe the structural phase transition as the temperature increases under the reducing conditions. In similar topotactic oxides, it has been found that the structural phase transition copes with the evolution of the electronic structure [22–25]. We conduct XAS measurements to collect other evidence of the oxygen-driven phase transitions. XAS measurements are carried out with as-grown P-SFCO and reduced BM-SFCO, which is annealed under N_2 conditions. Figures 2(a) and 2(b) show the XAS spectra of the Fe L edge and Co L edge of the P-SFCO and the BM-SFCO we obtain in the total electron yield (TEY) mode. It is expected that the number of electrons in the transition metals of BM-SFCO are greater than the number of electrons in P-SFCO. This can be demonstrated by XAS of transition metal L edges, which is a sensitive probe for changes in the valence state. In the Fe L edge in Fig. 2(a), from the comparison of each L edge spectrum, the change is due to changes of the oxygen content in SFCO thin films. Both Fe L edge spectra have doubletlike structures, which are typically seen in $SrFeO_x$ and $La_{1-x}Sr_xFeO_3$ [22,25]. The doublet shape depends on hole doping and/or oxygen deficiencies. As can be been in Fig. 2(a), each L_2 edge consists of two peaks. One peak at the lower energy can be considered as a t_{2g} state, while the peak at the higher energy can be considered as an e_g state [26–28]. It is easily seen that the relative intensity of the e_g state is decreased by the reduction process, since holes in the e_g state are replaced by electrons. The decrease of the relative intensity is triggered by the gain of electrons in the e_g state, which means that there is a loss of oxygen in the P-SFCO. As we have confirmed with real-time XRD, when oxygen is released from the film, the number of electrons in Fe increases. The increase of electrons leads to the decrease of empty orbitals in the e_g state. This reduces the probability of exciting electrons from the $2p$ level to the $3d$ e_g level. This results in a decrease in the intensity of the peak corresponding to the e_g level. We compared our results with M. Abbate *et al.* [22] to confirm the change in the e_g level. In our results, we clearly observe the inversion of peak intensity on reduction. In addition, we calculate the integrated peak intensities of e_g (I_{eg}) and t_{2g} (I_{t2g}) by the peak deconvolution of each spectrum. We calculate $I_{eg}/(I_{eg}+I_{t2g})$ to see the relative changes in intensity. It is clearly seen that the value changes from 0.89 to 0.73. Through the Fe L_2 edge spectrum analysis, we can confirm that the valence state of

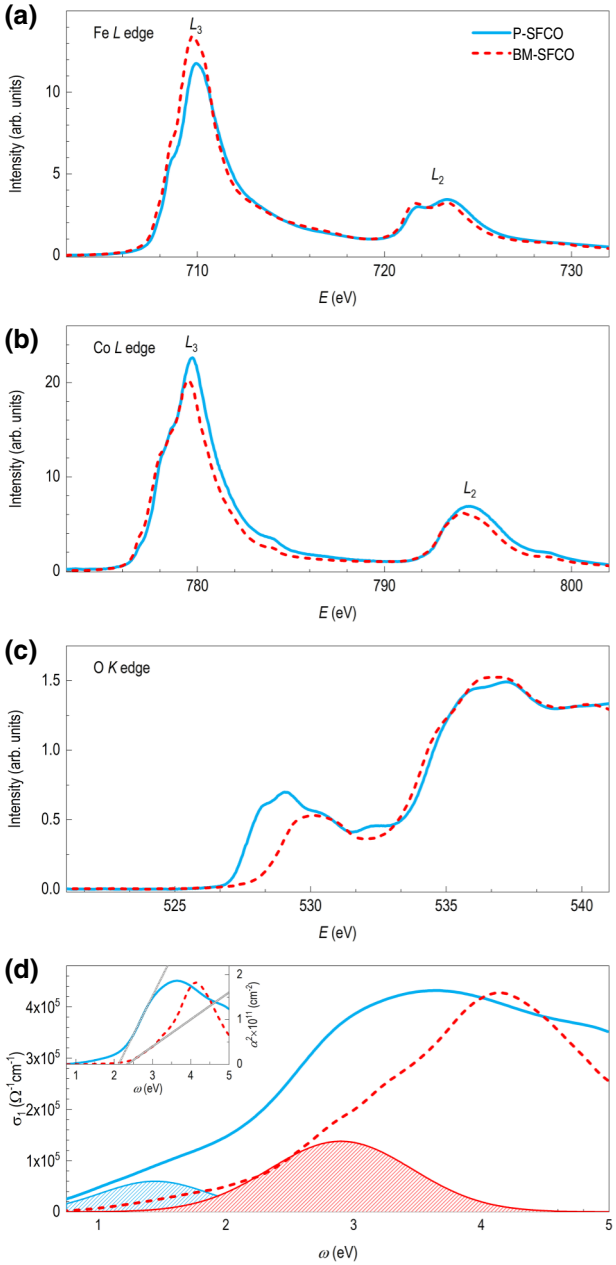

FIG. 2. (a) Fe L edge spectra, (b) Co L edge spectra, and (c) O K edge spectra of P-SFCO and BM-SFCO films by XAS. (d) Optical conductivity spectra of the as-grown P-SFCO and BM-SFCO thin films. The differences in optical conductivity spectra can be clearly seen. The inset shows the difference in extracted direct-optical band gap energies.

Fe is reduced through the reducing condition. This result is consistent with previous results from ferrites [22,25]. Even though the amount of Co is much smaller than the amount of Fe, we can observe the appreciable changes in the spectra by viewing the oxygen loss. The Co L edge is shown in Fig. 2(b). We can confirm the lower shift of Co L edges upon the reduction. We quantitatively confirm the value of the lower shift identified on the Co L edge based on previous studies. We compare the results of L. Karvonen *et al.* [29] to confirm the change in the Co valence state. When comparing the as-grown P-SFCO with the BM-SFCO, the lower shift of the Co L edge measured by XAS is 0.25 eV, which means that the valence state of Co decreases by 0.25. We qualitatively determine the Fe L edge measurement and quantitatively analyze the Co L edge to show that the low temperature annealing in the N_2 condition is a reduction.

To see the direct evidence of changes in the oxygen content of SFCO thin films in reduction, O K edge spectra are additionally taken [Fig. 2(c)]. It is well known that the prepeak in the O K edge spectrum is related to the hybridization between transition metals $3d$ and O $2p$ orbitals [9,25,29]. The prepeak intensity often reflects the oxygen content. The spectrum from BM-SFCO shows a weak prepeak, while that of the P-SFCO shows a prepeak with a relatively high intensity. In addition to the intensities, the overall shapes of the prepeak from the BM-SFCO and the P-SFCO are similar to the cases from $SrCoO_x$, $SrFeO_x$, and $La_{1-x}Sr_xFeO_3$ [22,25,29]. Possibly due to the B site content, the overall changes in shape are similar to the changes in the $SrFeO_x$ ($x = 2.48$–2.68) case. New peaks are shown in Fig. 2(c). Through this, we are able to confirm that the oxygen actually escapes via the reduction reaction. Those changes in the samples are strong evidence of the reduced oxygen content in the film after exposing it to N_2 gas at a low temperature. Finally, from the O K edge spectrum, an unoccupied state near the Fermi level is possibly visualized [30–32]. It should be pointed out that the oxidation prepeak starts at the lower energy. This reflects the shift of the DOS of the empty band toward the Fermi level. This implies the possible reduction of the band gap upon oxidation. Figure 2(d) shows the optical conductivities of two films obtained by spectroscopic ellipsometry. From the peak deconvolution, four distinct peaks are shown. These peaks are categorized into two groups. α and β are dominant in the spectrum of the P-SFCO film, while γ and δ are dominant in the spectrum of the BM-SFCO thin film. Among the transition features, the transition at the lowest energy from the P-SFCO is at 1.4 eV. However, the peak position at the lowest energy from the BM-SFCO is located at a much higher energy. The peak of γ is at 2.9 eV. The clearly different peak features of P-SFCO and BM-SFCO infer a possible difference in band gap energy in these two oxides. The absorption coefficient, a, is determined using k from our spectroscopic ellipsometry data to extract the optical band gap. The absorption coefficient is scaled as a^2 to extract the direct band gap energy as shown in the inset of Fig. 2(d). From the plots, we can deduct that the band gap energy is about 2.6 eV at BM-SFCO and 2.1 eV as a maximum at P-SFCO, respectively.

After confirming structural and electronic phase transitions from Figs. 1 and 2, we investigate the reversibility of the phase transition. Real-time XRD measurements are conducted at 375 °C in Fig. 3(a). Because we ramp up the temperature in N_2, the film is initially in the brownmillerite structure. The structure is maintained and there is no structural degradation at 375 °C, as can be seen in Figs. 1(b) and 1(c). We change the gas environment from a reducing condition to an oxidizing condition by putting dry air into the heater. We immediately observe the formation of new diffraction patterns with the peaks corresponding to the perovskite structure. This indicates the phase coexistence of both P-SFCO and BM-SFCO. After about 25 min, full phase conversion to the P-SFCO is complete. After confirming no further phase transformation, we start to change the gas type back to N_2. Lattice expansion immediately starts, but no vacancy-ordered structure is observed. This indicates an immediate loss of oxygen in the film. However, with a continued N_2 supply, it reverts back to BM-SFCO. This confirms a reversible redox-driven topotactic phase transition. An additional reversibility test is performed and can be found in Fig. S1. [33]. From the test, it is obvious that the topotactic phase transition is reversible. Note that this change leads to a change of the optical band gap. We confirm the phase transition through real-time

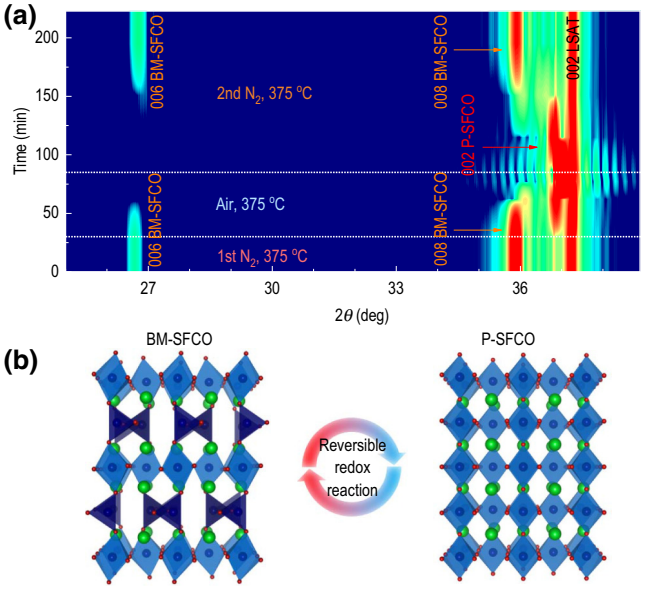

FIG. 3. (a) Gas-type-dependent real-time XRD θ-2θ measurement at 375 °C. (b) Schematic diagram of reversible redox reaction in SFCO.

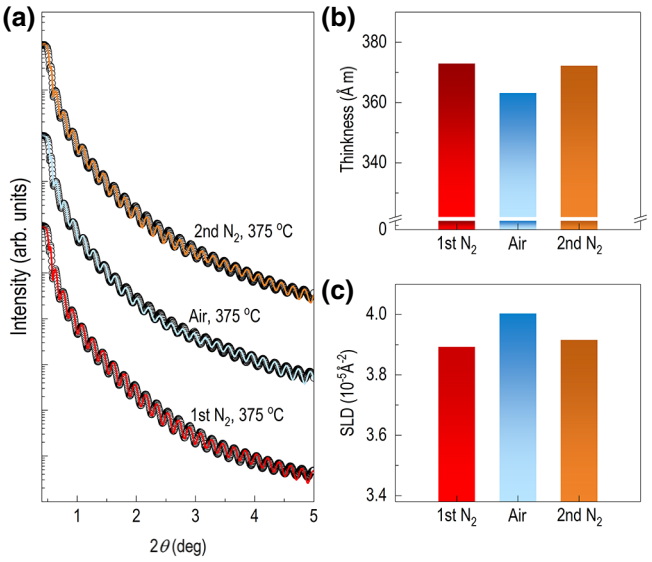

FIG. 4. (a) Gas-type-dependent x-ray reflectivity at 375 °C. Each red tone (P-SFCO) and blue tone (BM-SFCO) line shows experimental data and black circles show the simulated results. (b),(c) show changes in thickness and electron SLD values for SFCO layers under each condition, respectively.

XRD at atmospheric pressure. As shown in Fig. 3(b), initially, the octahedra and tetrahedral structures are stacked in the brownmillerite structure and show a half-order peak on XRD. When oxygen enters a part of the tetrahedra and the boundary of each layer becomes blurred, the half-order peak is not observed on the XRD. After changing back to the reducing condition, a structural phase transition back to brownmillerite takes place. This gives weight to our arguments that the transition occurs because of the Gibbs energy difference. The smaller difference is likely to the main driver for this reversibility.

After getting evidence of an oxygen-mediated phase transition, we additionally perform reflectivity measurements to determine what other parameters can be changed in these reversible transitions . Real-time XRR measurements are also performed by changing the gas in the following manner: N_2, air, and N_2. Figure 4(a) shows the reflectivity curves and there are two differences: the change of the critical angle and the interval between fringes. The critical angle is related to the density of the material. The interval between fringes is related to the thickness of the layer. We fit the data with the GenX [34] to check the thickness, roughness, and density of the SFCO film upon the phase transition. The fitted data are included in Figs. 4(b) and 4(c). Even though changes of the lattice constant according to the oxygen content were well known [35–40], the total thickness changes as the oxygen content changes have not been explored. In addition, the XRR can be a sensitive probe to show any signature of unreacted layers or chemically different layers along the depth direction [41]. This can be seen from additional modulation in the XRR spectra. We analyze our reflectivity data and all the data show Kiessig fringes without any modulation, which demonstrates that redox reactions are taking place through the entire films. From the fitting, it is confirmed that the total thickness also changes with gas type. As can be seen in Fig. 4(b), SFCO in N_2 have a thickness of 37.3 nm. With the lattice constant, we see that the BM-SFCO consists of about 93 layers. Interestingly, the calculation of the number of layers by XRR and XRD during redox reactions results in 93 layers, which demonstrates that the reactions take place in the entire volume as well as confirming there is no loss of the elements during the reactions. After putting in air, it is clearly seen that the thickness decreases to 36.3 nm. In perovskite, oxygen intercalation leads to the reduced unit cell volume. This fact is clearly shown in the reduction of the total thickness. After the intercalation, we put N_2 back into the heater and the total thickness changes back to 37.2 nm. In addition, we extract the changes of electron scattering length density (SLD) under the gas condition. Since the SLD is closely related to physical density, this is another indication of oxygen insertion or desorption. In Fig. 4(c), as we expect, more oxygen in the lattices results in a higher SLD. We check the thickness, roughness, and density of the fittings, and find that there is no abnormality when the different data sets show the change of the oxygen content.

IV. CONCLUSIONS

In conclusion, we clearly observe redox-driven nanoscale topotactic transformations between electronically, structurally, and chemically distinct SFCO phases at low temperature. The phase transition can occur at sufficiently low temperature as well as under the flow of different gas species, as shown by real-time x-ray scattering techniques. From the *ex situ* characterization, we unambiguously observe that the two phases are chemically and electronically distinct from x-ray absorption spectroscopy and spectroscopic ellipsometry. These reversible redox-driven topotactic transformations at low temperature and atmospheric pressure indicate that SFCO can potentially be a cathode material for low-temperature solid-oxide fuel cells. In addition, the ease of changing the oxygen content-driven phase transition via different gas flows will be a viable tool to tune the physical properties as well as an important strategy for low-temperature mixed electronic and ionic conduction in energy applications.

ACKNOWLEDGMENTS

This work was supported by the National Research Foundation of Korea (NRF) grant funded by the Korea government (MSIT) through GCRC-SOP (No. 2011-0030013). This research was also supported by the Basic Science Research Program through the NRF

funded by the Ministry of Education (Grant No. NRF-2015R1D1A1A02062175).

[1] M. Uehara, S. Mori, C. H. Chen, and S. W. Cheong, Percolative phase separation underlies colossal magnetoresistance in mixed-valent manganites, Nature **399**, 560 (1999).

[2] J. Mannhart and D. G. Schlom, Semiconductor physics: The value of seeing nothing, Nature **430**, 620 (2004).

[3] J. Wang *et al.*, Epitaxial $BiFeO_3$ multiferroic thin film heterostructures, Science **299**, 1719 (2003).

[4] E. Dagotto, Complexity in strongly correlated electronic systems, Science **309**, 257 (2005).

[5] N. Reyren *et al.*, Superconducting interfaces between insulating oxides, Science **317**, 1196 (2007).

[6] H. Y. Hwang, Y. Iwasa, M. Kawasaki, B. Keimer, N. Nagaosa, and Y. Tokura, Emergent phenomena at oxide interfaces, Nat. Mater. **11**, 103 (2012).

[7] E. Dagotto, T. Hotta, and A. Moreo, Colossal magnetoresistant materials: The key role of phase separation, Phys. Rep.-Rev. Sec. Phys. Lett. **344**, 1 (2001).

[8] S. V. Kalinin and N. A. Spaldin, Functional ion defects in transition metal oxides, Science **341**, 858 (2013).

[9] H. Jeen *et al.*, Reversible redox reactions in an epitaxially stabilized $SrCoO_x$ oxygen sponge, Nat. Mater. **12**, 1057 (2013).

[10] H. Jeen, W. S. Choi, J. W. Freeland, H. Ohta, C. U. Jung, and H. N. Lee, Topotactic phase transformation of the brownmillerite $SrCoO_{2.5}$ to the perovskite $SrCoO_{3-\delta}$, Adv. Mater. **25**, 3651 (2013).

[11] Q. H. Zhang *et al.*, Atomic-resolution imaging of electrically induced oxygen vacancy migration and phase transformation in $SrCoO_{2.5-\sigma}$, Nat. Commun. **8**, 104 (2017).

[12] J. Jeong, N. Aetukuri, T. Graf, T. D. Schladt, M. G. Samant, and S. S. P. Parkin, Suppression of metal-insulator transition in VO_2 by electric field-induced oxygen vacancy formation, Science **339**, 1402 (2013).

[13] N. P. Lu *et al.*, Electric-field control of tri-state phase transformation with a selective dual-ion switch, Nature **546**, 124 (2017).

[14] Q. Y. Lu and B. Yildiz, Voltage-controlled topotactic phase transition in thin-film $SrCoO_x$ monitored by in situ X-ray diffraction, Nano Lett. **16**, 1186 (2016).

[15] H. Yoon, M. Choi, T. W. Lim, H. Kwon, K. Ihm, J. K. Kim, S. Y. Choi, and J. Son, Reversible phase modulation and hydrogen storage in multivalent VO_2 epitaxial thin films, Nat. Mater. **15**, 1113 (2016).

[16] J. Maier, Nanoionics: Ion transport and electrochemical storage in confined systems, Nat. Mater. **4**, 805 (2005).

[17] D. B. Meadowcroft, Low-cost oxygen electrode material, Nature **226**, 847 (1970).

[18] E. D. Wachsman and K. T. Lee, Lowering the temperature of solid oxide fuel cells, Science **334**, 935 (2011).

[19] S. Inoue, M. Kawai, N. Ichikawa, H. Kageyama, W. Paulus, and Y. Shimakawa, Anisotropic oxygen diffusion at low temperature in perovskite-structure iron oxides, Nat. Chem. **2**, 213 (2010).

[20] A. Khare *et al.*, Topotactic metal-insulator transition in epitaxial $SrFeO_x$ thin films, Adv. Mater. **29**, 1606566 (2017).

[21] N. Ichikawa, M. Iwanowska, M. Kawai, C. Calers, W. Paulus, and Y. Shimakawa, Reduction and oxidation of $SrCoO_{2.5}$ thin films at low temperatures, Dalton Trans. **41**, 10507 (2012).

[22] M. Abbate *et al.*, Controlled-valence properties of $La_{1-x}Sr_xFeO_3$ and $La_{1-x}Sr_xMnO_3$ studied by soft-x-ray absorption spectroscopy, Phys. Rev. B **46**, 4511 (1992).

[23] M. Abbate, G. Zampieri, J. Okamoto, A. Fujimori, S. Kawasaki, and M. Takano, X-ray absorption of the negative charge-transfer material $SrFe_{1-x}Co_xO_3$, Phys. Rev. B **65**, 7 (2002).

[24] J. Okamoto *et al.*, Antiferromagnetic-to-ferromagnetic transition induced by diluted Co in $SrFe_{1-x}Co_xO_3$: Magnetic circular x-ray dichroism study, Phys. Rev. B **71**, 5 (2005).

[25] V. R. Galakhov, E. Z. Kurmaev, K. Kuepper, M. Neumann, J. A. McLeod, A. Moewes, I. A. Leonidov, and V. L. Kozhevnikov, Valence band structure and X-ray spectra of oxygen-deficient ferrites $SrFeO_x$, J. Phys. Chem. C **114**, 5154 (2010).

[26] S. Erat, H. Wadati, F. Aksoy, Z. Liu, T. Graule, L. J. Gauckler, and A. Braun, Iron-resonant valence band photoemission and oxygen near edge x-ray absorption fine structure study on $La_{1-x}Sr_xFe_{0.75}Ni_{0.25}O_{3-\delta}$, Appl. Phys. Lett. **97**, 124101 (2010).

[27] E. J. Moon, Y. J. Xie, E. D. Laird, D. J. Keavney, C. Y. Li, and S. J. May, Fluorination of epitaxial oxides: Synthesis of perovskite oxyfluoride thin films, J. Am. Chem. Soc. **136**, 2224 (2014).

[28] F. M. F. Degroot, Ph.D. thesis, University of Nijmegen, 1991.

[29] L. Karvonen, M. Valkeapaa, R. S. Liu, J. M. Chen, H. Yamauchi, and M. Karppinen, O-*K* and Co-*L* XANES study on oxygen intercalation in perovskite $SrCoO_{3-\delta}$, Chem. Mat. **22**, 70 (2010).

[30] F. M. F. Degroot, X-ray absorption of transition metal oxides: An overview of the theoretical approaches, J. Electron Spectrosc. Relat. Phenom. **62**, 111 (1993).

[31] F. M. F. Degroot, J. Faber, J. J. M. Michiels, M. T. Czyzyk, M. Abbate, and J. C. Fuggle, Oxygen 1*s* x-ray absorption of tetravalent titanium oxides: A comparison with single-particle calculations, Phys. Rev. B **48**, 2074 (1993).

[32] D. D. Sarma, N. Shanthi, and P. Mahadevan, Electronic excitation spectra from ab initio band-structure results for $LaMO_3$ ($M = $ Cr,Mn,Fe,Co,Ni), Phys. Rev. B **54**, 1622 (1996).

[33] See Supplemental Material at http://link.aps.org/supplemental/10.1103/PhysRevApplied.10.054035 for the reversibility of redox reactions.

[34] M. Bjorck and G. Andersson, GenX: An extensible X-ray reflectivity refinement program utilizing differential evolution, J. Appl. Crystallogr. **40**, 1174 (2007).

[35] Y. Takeda, K. Kanno, T. Takada, O. Yamamoto, M. Takano, N. Nakayama, and Y. Bando, Phase relation in the oxygen nonstoichiometric system, $SrFeO_x$ ($2.5 \leq x \leq 3.0$), J. Solid State Chem. **63**, 237 (1986).

[36] A. Nemudry, P. Weiss, I. Gainutdinov, V. Boldyrev, and R. Schollhorn, Room temperature electrochemical redox

reactions of the defect perovskite $SrFeO_{2.5+x}$, Chem. Mater. **10**, 2403 (1998).

[37] M. Schmidt and S. J. Campbell, In situ neutron diffraction study (300–1273 K) of non-stoichiometric strontium ferrite $SrFeO_x$, J. Phys. Chem. Solids **63**, 2085 (2002).

[38] A. Nemudry, P. Rudolf, and R. Schöllhorn, Topotactic electrochemical redox reactions of the defect perovskite $SrCoO_{2.5+x}$, Chem. Mater. **8**, 2232 (1996).

[39] H. Evenrud and S. Stolen, Redox thermochemistry of $SrFe_{1-x}Co_xO_{3-\delta}$, J. Therm. Anal. Calorim. **69**, 795 (2002).

[40] Y. W. Long, Y. Kaneko, S. Ishiwata, Y. Tokunaga, T. Matsuda, H. Wadati, Y. Tanaka, S. Shin, Y. Tokura, and Y. Taguchi, Evolution of magnetic phases in single crystals of $SrFe_{1-x}Co_xO_3$ solid solution, Phys. Rev. B **86**, 064436, (2012).

[41] S. Singh, M. R. Fitzsimmons, T. Lookman, J. D. Thompson, H. Jeen, A. Biswas, M. A. Roldan, and M. Varela, Magnetic Nonuniformity and Thermal Hysteresis of Magnetism in a Manganite Thin Film, Phys. Rev. Lett. **108**, 077207 (2012).